WATER RESOURCES BULLETIN
VOL. 31, NO. 3 AMERICAN WATER RESOURCES ASSOCIATION JUNE 1995

RASTER-BASED HYDROLOGIC MODELING OF SPATIALLY-VARIED SURFACE RUNOFF[1]

Pierre Y. Julien, Bahram Saghafian, and Fred L. Ogden[2]

ABSTRACT: The proliferation of watershed databases in raster Geographic Information System (GIS) format and the availability of radar-estimated rainfall data foster rapid developments in raster-based surface runoff simulations. The two-dimensional physically-based rainfall-runoff model CASC2D simulates spatially-varied surface runoff while fully utilizing raster GIS and radar-rainfall data. The model uses the Green and Ampt infiltration method, and the diffusive wave formulation for overland and channel flow routing enables overbank flow storage and routing. CASC2D offers unique color capabilities to display the spatio-temporal variability of rainfall, cumulative infiltrated depth, and surface water depth as thunderstorms unfold. The model has been calibrated and independently verified to provide accurate simulations of catchment response to moving rainstorms on watersheds with spatially-varied infiltration. The model can accurately simulate surface runoff from flashfloods caused by intense thunderstorms moving across partial areas of a watershed.
(KEY TERMS: hydrologic model; surface runoff; GIS hydrology; radar hydrology; flashfloods; moving rainstorms.)

INTRODUCTION

Recent developments in Geographic Information System (GIS) and micro-computer technology enhance our capabilities to handle large databases describing the detailed spatial configuration of land-surface. As opposed to a vector-based format, a raster-based GIS offers a practical method for storing land-surface characteristics with digital values of a parameter on square grid elements. A watershed is divided into square cells of specified grid size, and a single value of a land-surface parameter is assigned to each cell. Land-surface characteristics such as elevation, soil type, and land-use are obtained by field sampling (in the case of soil classification) or remote sensing (photogrammetry for elevation, satellite imagery for land-use classification).

There is an extensive effort in many states to establish a raster database of soil classification with 200 m spatial resolution. The U.S. Geological Survey maintains an on-line Internet accessible Digital Elevation Model (DEM) of raster elevations for the entire U.S., primarily at a 90 m horizontal resolution and 1 m vertical resolution. Advances are also being made in the field of rainfall remote sensing, which allow widespread estimation of rainfall rates at spatial resolutions ranging from 1 to 4 km. The U.S. National Weather Service is presently updating its weather radar capabilities with the deployment of over 120 WSR-88D radars, known as NEXRAD (Klazura and Imy, 1993). The NEXRAD precipitation processing system produces hourly accumulated rainfall estimates on a 4 x 4 km grid. Furthermore, there are several regions covered by research weather radars which can provide rainfall rate estimates at spatial and temporal resolutions as fine as 1 km every 5 minutes.

Physically-based distributed hydrologic models typically employ field-measured or remotely-sensed values describing the spatially-varied nature of watershed topography, soils, vegetation, drainage networks, and rainfall. These variables are used as input to numerical algorithms based on the physics of infiltration and overland and channel flow to model the transient response of a watershed. Two-dimensional physically-based numerical models are gaining popularity among hydrologists concerned with simulating the non-linear response of watersheds to spatially-varied rainfall and infiltration. Models of this type

[1]Paper No. 94057 of the *Water Resources Bulletin*. **Discussions are open until February 1, 1996.**
[2]Respectively, Associate Professor of Civil Engineering, Engineering Research Center, Colorado State University, Fort Collins, Colorado 80523; formerly at the Civil Engineering Department, Engineering Research Center, Colorado State University, Fort Collins, Colorado; and Assistant Professor, Department of Civil Engineering, University of Connecticut, Storrs, Connecticut (formerly at Colorado State University).

incorporate a description of watershed and rainfall spatial variability at resolutions considerably finer than contemporary lumped parameter models.

Abbott *et al.* (1986) reported on the structure of a physically-based distributed modeling system named Système Hydrologique Européen (SHE), which uses modular construction for the addition of new components. Two-dimensional overland flow routing is performed using an explicit finite difference scheme, while one-dimensional channel flow routing is carried out by an implicit method. Other SHE components include interception, evapotranspiration, saturated and unsaturated zone flows, and snowmelt. Abbott *et al.* (1986) predicted that technological advances in remote sensing and radar measurement would enhance data handling for SHE.

More recent developments in two-dimensional hydrodynamic modeling of runoff routing include, among others, Zhang and Cundy (1989) and James and Kim (1990). The first model considers the spatial variation in hillslope physical characteristics and numerically solves the general hydrodynamic equations of continuity and motion using a finite difference scheme. The second model simulates uncoupled overland and channel flow routing for a single storm event. Excess rainfall calculated by the Green-Ampt infiltration equation is routed as overland flow using a two-dimensional diffusive wave implicit scheme.

Two-dimensional overland flow modeling using the finite element approach was reported by Goodrich *et al.* (1991). They developed a method using the kinematic wave equations approximated in space by finite elements on a topographic triangular irregular network (TIN). The resulting ordinary differential equations were then solved in time via finite differences. Goodrich *et al.* (1991) hinted at the need for further research to incorporate infiltration and refinement of their numerical techniques. Marcus (1991) developed a distributed finite element overland flow model to simulate moving rainstorms event on natural watersheds subdivided by quadrilateral elements. A two-dimensional kinematic wave approximation combined with the Manning resistance equation was formulated to compute the surface runoff. The model was linked to a one-dimensional full dynamic channel network model (Choi and Molinas, 1993) for the simulation of flashfloods in semi-arid watersheds.

While models exist which use a format consistent with recent developments in GIS and rainfall remote sensing technologies, none have been developed expressly for the purpose of fully utilizing raster-based GIS and radar capabilities. Additionally, none of the above-mentioned models include capabilities for visualizing the spatial variability of rainfall, surface water, or cumulative infiltrated depth during a simulation.

Data manipulation and visualization capabilities gained in GIS-hydrologic model linkage were demonstrated by Cline *et al.* (1989) and Vieux (1991), who linked distributed process-based models with GIS. Past efforts and trends in the application of GIS for hydrologic analysis, comparison and grid-, TIN-, and contour-based GIS, and the use of remotely sensed data in GIS and hydrologic modeling were extensively reviewed by DeVantier and Feldman (1993).

This paper describes the distributed watershed model CASC2D. CASC2D is fully compatible with a raster-based GIS and raster weather radar rainfall estimates, and it simulates Hortonian surface runoff from moving rainstorms in semi-arid and humid regions. The objectives for developing this model include the need for: (a) spatial data handling linked with raster-based GIS; (b) hydrologic modeling linked with remotely sensed rainfall data; (c) accurate flash-flood simulation for intense thunderstorms moving across partial areas of a watershed; and (d) graphical display capability for educational, scientific, and diagnostic applications which illustrate the spatio-temporal variability of rainfall, infiltration, and surface water depth.

This paper demonstrates the capabilities and limitations of CASC2D with emphasis on model formulation, features, calibration, verification, independent testing, and numerical stability. Two examples illustrate the capabilities: (a) the calibration run with rainfall data from a dense raingauge network, and (b) research results using dual-Doppler weather radar.

MODEL FORMULATION

CASC2D is designed to operate on watershed data discretized into square raster elements of desired spatial resolution. The selection of an appropriate grid size for simulations is not a trivial matter. In selecting a grid size, the user must balance between accuracy, data availability, and computational effort. The availability and accuracy of the data used for calibration and verification should also be considered. Values of model grid size used with CASC2D to date range from 30 m to 800 m, with typical values between 100 and 200 m. Small grid sizes are used when the spatial variability of relevant parameters is known in detail. Larger grid sizes may be preferred when the spatial variability of watershed characteristics is not significant or when computational efficiency is a concern, such as simulations of very large watersheds or large numbers of storms – e.g., Monte-Carlo simulations. A raster-based GIS proves to be extremely useful when data sets need to be rescaled to larger grid resolutions.

The geographic region which bounds the watershed is divided into raster cells of size W. Each grid cell is identified by its row and column numbers (j,k). A mask map is developed which describes whether or not a particular grid cell lies within the boundary of the watershed. The mask map resembles a matrix where 1 denotes a grid cell within the watershed, while a value of 0 indicates that the grid cell lies outside the watershed. Cells on the boundary are considered inside the watershed if more than 50 percent of their area is contained within the watershed boundary line.

The following sections contain algorithmic descriptions of the three main components of CASC2D. These main components include: infiltration, overland flow routing, and channel routing.

Infiltration

The Green and Ampt equation is used to determine infiltration rates, assuming the soils are homogeneous, deep, and well-drained within each grid cell (Rawls *et al.*, 1983):

$$f = K\left(1+\frac{H_f M_d}{F}\right) \tag{1}$$

where f = infiltration rate; K = hydraulic conductivity; H_f = capillary pressure head at the wetting front; M_d = soil moisture deficit equal to $(\theta_e-\theta_i)$; θ_e = effective porosity equal to $(\phi-\theta_r)$; ϕ = total soil porosity; θ_r = residual saturation; θ_i = initial soil moisture content; and F = total infiltrated depth. The degree of initial soil saturation S in percent is given by $S = \theta_i/\theta_e$. The head due to surface depth is neglected because H_f is typically much greater than the overland flow depth. Based on soil textural classification, Rawls *et al.* (1983) provided average values for the Green and Ampt parameters.

Starting from an initial surface water depth, usually zero at the beginning of a storm, the rainfall depth during the time step Δt is first added to the surface water depth. The infiltration rate is then calculated for each grid cell from Equation (1). The actual infiltration rate is taken as the lesser of the infiltration capacity and the maximum available rate calculated by dividing the surface water depth by the time step. Solving Equation (1) for the middle of the time step yields:

$$f^{t+\Delta t/2} = \frac{1}{2\Delta t}\left\{\left(K\Delta t - 2F^t\right)+\left[\left(K\Delta t - 2F^t\right)^2 + 8\left(KF^t + KH_f M_d\right)\Delta t\right]^{1/2}\right\} \tag{2}$$

in which Δt = time step, and the superscripts correspond to time. This model essentially simulates the Hortonian surface runoff mechanism. There is no provision for the recovery of infiltration capacity between storms because of soil-moisture redistribution. This has little effect on single storm simulations but should be reset for multiple storm simulations. At this time, this formulation does not include provisions for sub-surface storage or routing. For this reason, the CASC2D simulates surface runoff from watersheds; baseflow contributions from subsurface flow should be added when appropriate.

The required input data for the infiltration routine includes raster maps of textural classification (Rawls *et al.* 1983) and initial soil moisture deficit. These data may be derived from field estimates or manually digitized county soil surveys at the desired spatial resolution or obtained from the Soil Conservation Service within a particular state in raster GIS format.

Overland Flow

A two-dimensional explicit finite difference formulation was selected to model overland flow. Topographical data from a DEM are assigned to each raster grid cell as conceptualized in Figure 1. This figure illustrates the description of topography within CASC2D and is consistent with raster GIS formulations. In general, each raster cell is assumed a homogeneous unit with one representative value of any hydraulic or hydrologic parameter (e.g., hydraulic conductivity, roughness coefficient, elevation, etc).

The Saint-Venant equations of continuity and momentum describe the physics of gradually-varied overland flow. The two-dimensional continuity equation in partial differential form is:

$$\frac{\partial h}{\partial t}+\frac{\partial q_x}{\partial x}+\frac{\partial q_y}{\partial y} = i_e \tag{3}$$

where h = surface flow depth; q_x = unit discharge in x-direction; q_y = unit discharge in y-direction; i_e = excess rainfall equal to (i-f); i = rainfall intensity; x and y = rectangular coordinates; and t = time.

Application of a first order approximation to the continuity equation for element (j,k) results in:

$$h^{t+\Delta t}(j,k) = h^t(j,k) + i_e\Delta t - \left[\frac{q_x{}^t(k \to k+1) - q_x{}^t(k-1 \to k)}{W} + \frac{q_y{}^t(j \to j+1) - q_y{}^t(j-1 \to j)}{W}\right]\Delta t \quad (4)$$

where $h^{t+\Delta t}(j,k)$ and $h^t(j,k)$ denote flow depths at element (j,k) at time t+ Δt and t, respectively; i_e is the average excess rainfall rate over one time step beginning from time t; $q_x{}^t(k \to k+1)$ and $q_x{}^t(k-1 \to k)$ describe unit flow rates in x-direction at time t, from (j,k) to (j,k+1), and from (j,k-1) to (j,k), consecutively; likewise $q_y{}^t(j \to j+1)$, $q_y{}^t(j-1 \to j)$ denote unit flow rates in y-direction at time t, from (j,k) to (j+1,k), and from (j-1,k) to (j,k), respectively; and W = grid size.

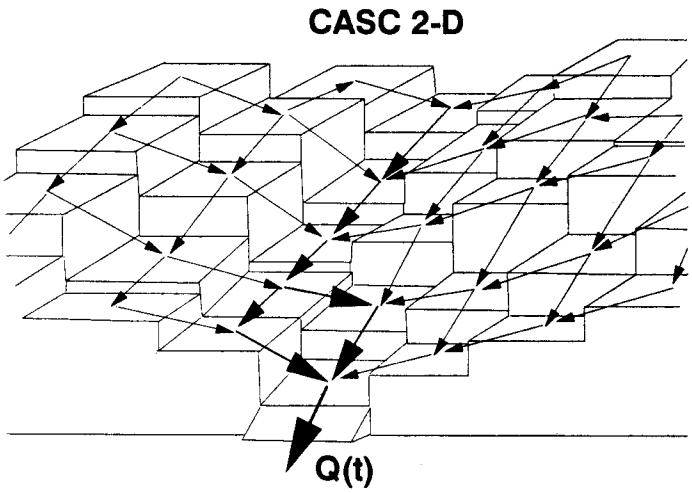

Figure 1. Topographical Representation in Overland Flow Routing Scheme.

The momentum equations in the x and y directions may be derived by relating the net forces per unit mass to flow acceleration. The diffusive wave approximation of the momentum equation in the x-direction is:

$$S_{fx} = S_{ox} - \frac{\partial h}{\partial x} \quad (5)$$

where S_{fx} = friction slope in the x-direction; and S_{ox} = land surface slope in the x-direction. With reference to Figure 1, the land surface slope in the x- and y-directions is calculated as the difference in elevation between two adjacent cells divided by the grid size, W.

The unit discharge at any position and any time depends primarily upon the flow direction, which is determined by the sign of the friction slope. For example, in the x-direction, first the friction slope based on the diffusive wave approximation is computed as:

$$S_{fx}{}^t(k-1 \to k) = S_{ox}(k-1 \to k) - \frac{h^t(j,k) - h^t(j,k-1)}{W} \quad (6)$$

in which the bed slope is given by:

$$S_{ox}(k-1 \to k) = \frac{E(j,k-1) - E(j,k)}{W} \quad (7)$$

where E represents the ground surface elevation of the element, and the arrows imply the computational direction. From the three equations of continuity and momentum, five hydraulic variables must be determined. Therefore, a resistance law in terms of depth-discharge relationship is required such as:

$$q_x = \alpha_x h^\beta \quad (8)$$

where α_x varies with the derivative of depth in diffusive formulation and β is a constant. Both α_x and β depend on flow regime – i.e., laminar or turbulent.

For turbulent flow over a rough boundary, the Manning resistance equation, in SI units, is used:

$$\alpha_x = \frac{S_{fx}{}^{1/2}}{n}; \quad \beta = \frac{5}{3} \quad (9)$$

where n=Manning roughness coefficient. Notice that the parameter β remains constant while the coefficient α_x varies during a rainstorm simulation according to S_{fx} from Equation (6).

The calculated unit discharge for turbulent flow is then given by:

$$q_x{}^t(k-1 \to k) = \frac{1}{n(j,k-1)}\left[h^t(j,k-1)\right]^{5/3} \left[S_{fx}{}^t(k-1 \to k)\right]^{1/2} \quad \text{if} \quad S_{fx}{}^t(k-1 \to k) \geq 0 \quad (10)$$

$$q_x{}^t(k-1 \to k) = \frac{-1}{n(j,k)}\left[h^t(j,k)\right]^{5/3} \left[-S_{fx}{}^t(k-1 \to k)\right]^{1/2} \quad \text{if} \quad S_{fx}{}^t(k-1 \to k) < 0 \quad (11)$$

Equation (11) corresponds to a negative friction slope and negative unit discharge and therefore implies that the flow direction is actually from (j,k) to (j,k-1).

The flow rates in the y-direction are calculated based on the sign of the friction slopes in the y-direction. Backwater effects are handled in Equations (10), (11), and (4) whenever the sign of bed slope S_o and friction slope S_f happen to be opposite. Wherever microscale topography within a cell prevents the surface water from flowing after soil saturation, a retention storage depth specified for each cell causes ponding of surface water without runoff until the specified retention depth is exceeded.

Data requirements for the overland flow portion of CASC2D include raster maps of topography, retention storage depth, and surface roughness coefficient. The land-surface slope map is derived from the topographical map. Each of these raster maps may be generated either manually or with a raster GIS.

This formulation has several unique features. Firstly, it enables the simulation of run on, which occurs when surface runoff from one cell flows onto an adjacent cell where it is infiltrated. Secondly, the diffusive wave formulation allows flow on adverse slopes due to backwater effects. The upstream boundary condition for overland flow allows no inflow into the watershed across its boundary. The coupling of overland flow and channel flow is addressed in the next section.

Channel Flow

The one-dimensional diffusive wave formulation is applied to the following one-dimensional continuity equation:

$$\frac{\partial A_X}{\partial t} + \frac{\partial Q}{\partial x} = q_1 \qquad (12)$$

where A_x = channel flow cross section; Q = total discharge in the channel; and q_1 = lateral inflow rate per unit length, in (+) or out (–) of the channel. The application of the Manning resistance equation to the channel flow can be described as:

$$Q = \frac{1}{n} A_x R^{2/3} S_f^{1/2} \qquad (13)$$

where R = channel hydraulic radius; and S_f = channel friction slope. The solution of Equation (12) using Equations (13) and (6) is similar to Equation (4), although only in one-dimension.

Grid cells which contain channel segments are referred to as "drainage cells." The connectivity between the overland flow and channel network is specified by the user in a raster map. Channels are assumed to flow between the center of two successive drainage cells. The length of the channel segment between two successive drainage cells may be specified as a length other than the grid size to account for channel sinuosity or flow along the diagonal (relative to the grid directions) lines.

At each time step, overland flow is calculated to determine the net surface runoff discharge flowing into the drainage cells. The entire incoming flow exceeding a specified retention depth in drainage cells is treated as lateral inflow to the channel segments within those cells. Figure 2 shows a typical drainage cell containing a channel segment of width WCH, bankfull depth DCH, and water depth HCH. If HCH is less than DCH, all overland inflow to a drainage cell from adjacent overland cells is passed to the channel. However, when HCH exceeds DCH, overbank flow occurs onto the adjacent floodplain. During periods of overbank flow, the volume of water within each drainage cell is distributed between in-channel and floodplain compartments each time step with the assumption of an equal water surface elevation in the channel and on the floodplain. Once water leaves the channel and moves onto the floodplain, it is treated as overland flow and accordingly may interact with other neighboring overland cells, or infiltrate. As the flood wave in the channel recedes, water on the flood plain is returned to the channel, with the exception of the specified retention depth.

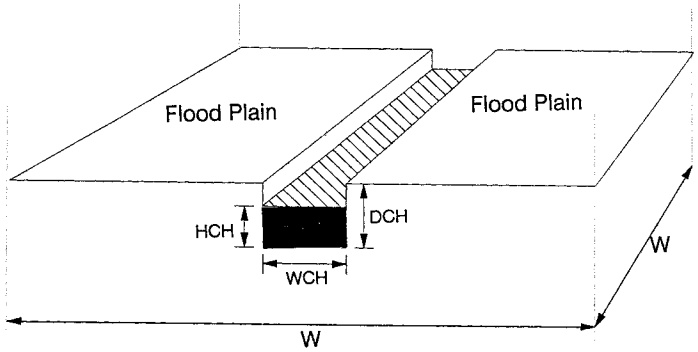

Figure 2. Typical Drainage Cell with Channel Cross Section.

The upstream boundary condition for first-order streams at the hillslope-channel interface is the overland flow rate entering the upstream drainage cells. The continuity equation and an equal water surface assumption serve as boundary conditions at channel junctions. At the watershed outlet the downstream boundary condition can be specified as: normal depth, weir or a stage vs. time relationship. Data requirements for the channel routing portion of CASC2D

include raster maps of drainage cell locations (connectivity), channel geometry (width, depth), and roughness coefficient (Manning n).

The diffusive wave channel routing formulation in CASC2D simulates backwater effects. This is particularly important in streams with very flat or adverse slopes. This formulation also allows flow over artificial barriers due to errors in DEM data or "digital dams" obstructing the flow in a wide cross-section. Surface water accumulates behind the barrier until the depth exceeds the barrier height and then spills over. Engineering judgement is required to remove, smooth, or filter errors in DEM data bases.

MODEL FEATURES

There are three specific features which enhance the applicability of CASC2D:

1. GIS Data Link – CASC2D operates on raster GIS-processed input data files (e.g., DEM, soil textural classification, land-use and land-cover data). To date, development has focused on the linkage of CASC2D with the public-domain Geographic Resources Analysis Support System (GRASS) GIS developed by the U.S. Army Construction Engineering Research Laboratories in Champaign, Illinois. The CASC2D-GRASS linkage was first demonstrated by Doe and Saghafian (1992), where GRASS capabilities were used to generate maps of land-surface disturbance at the Pinon Canyon Maneuver Site in Southern Colorado (Doe, 1992). CASC2D is ASCII-compatible with GRASS raster maps and conceptually compatible with any other raster-based GIS.

2. Moving Rainstorm Input Capability – There are three methods to input rainfall rates in CASC2D. These methods are spatially uniform rainfall rate of specified duration, rainfall time-series with constant temporal resolution at a number of rain gauges, or raster rainfall estimates with specified temporal resolution. Rainfall fields are interpolated from rainfall rates recorded by gauges located on or near the watershed using either Thiessen polygon or inverse distance squared techniques. Raster maps of rainfall rate from either weather radar (Ogden and Julien, 1994) or space-time rainfall model sources (Ogden and Julien, 1993) sources may be applied at a specified temporal resolution.

3. Graphical Display – One of the stated objectives for the development of CASC2D was the desire for visual interpretation of the rainfall-runoff process. GIS methods have allowed visual inspection of large geophysical, geological, and other datasets. The same display capability within a hydrologic modeling context is quite useful for educational, scientific, and diagnostic purposes. The graphical capabilities of CASC2D consist of a large window which is broken into several sub-windows. Each sub-window displays either a specified raster map, or a runoff hydrograph at a specified point in the watershed. Versions of the graphical display exist for both the MS-DOS and UNIX/X-Windows environments.

COMPONENT CALIBRATION/VERIFICATION

Several case studies to test the performance of CASC2D are reported in Julien and Saghafian (1991) and are summarized here. These test cases were used to assess the accuracy of individual components of CASC2D (i.e., overland flow routing, channel flow routing, and infiltration), as well as the combined performance of all components.

The overland flow routing component of CASC2D was tested against analytical solutions of the kinematic wave equation on the one-dimensional flow plane (Woolhiser, 1975) and converging plane (Woolhiser, 1969). Analytical solutions are available only for the kinematic wave situation, and despite the fact that CASC2D employs the diffusive wave formulation, the diffusive wave solution becomes identical to the kinematic wave on steeper slopes where backwater effects are negligible. In each of these two cases, the numerical solution provided by the CASC2D algorithm is identical to the analytical solution with the exception of slight numerical diffusion near the peak on the rising limb.

The CASC2D overland flow formulation was also compared with multiple experimental data sets reported by Dickinson *et al.* (1967) for an impervious butyl rubber converging plane, and by Schaake (1965) for the asphalt-covered Johns Hopkins University parking lot. The Manning roughness coefficient was used as the sole calibration parameter of the CASC2D overland flow algorithm. In this evaluation, one subset of each of the above data sets was used as a calibration data set, and the model was verified against the remaining data sets. CASC2D was calibrated on the magnitude of the peak discharge. Results from these calibrations/verifications are shown in Table 1, and they support the validity of the formulation. The average verification errors are 3 percent and –4.5 percent for the peak discharge and time to peak, while the average absolute values of the verification errors are 4.4 percent and 4.5 percent for the peak discharge and time to peak, respectively. The average calibration error on the runoff volume at the end of the

TABLE 1. Calibration/Verification of CASC2D Overland Flow Module with Experimental Datasets of Dickinson *et al.* (1967) and of Schaake (1965).

	Peak Discharge			Time to Peak			Runoff Volume (at end of observed data)		
	Observed m^3/s	Simulated m^3/s	Error %	Observed sec.	Simulated sec.	Error %	Observed m^3/s	Simulated m^3/s	Error %
Data Sets by Dickinson *et al.* (1967)									
Calibration Run	0.0035	0.0035	0.00	156	159	1.92	0.56	0.53	–5.36
Verification Run	0.0109	0.0116	6.42	121	112	–7.44	1.21	1.27	4.96
Data Sets by Schaake *et al.* (1965)									
Calibration Run (Storm #7)	0.0215	0.0215	0.00	426	438	2.82	14.4	13.3	–7.63
Verification Run (Storm #3)	0.0344	0.0351	1.97	1014	978	–3.55	18.8	19.9	5.85
Verification Run (Storm #13)	0.0654	0.0696	6.38	672	660	–1.79	37.6	43.7	16.22
Verification Run (Storm #18)	0.0277	0.0269	–2.85	702	666	–5.13	10.5	9.7	–7.62

observed data sets is –6.5 percent, while on the verification data sets it is 4.9 percent. Note that runoff volume was not considered a calibration requirement. The results in Table 1 indicate that there is a tendency to underestimate the time to peak by 4.5 percent. Otherwise, there are no obvious biases in the overland flow algorithm as evidenced by the signs on the error magnitudes with the peak discharge and runoff volume.

The channel routing algorithm was evaluated against the implicit full dynamic solution of the shallow water equations of motion developed by Choi and Molinas (1993). The explicit channel routine was found to be mass-conservative and accurate compared to the full-dynamic routing method. The performance of the Green and Ampt formulation used in CASC2D was compared with a numerical solution of Richards equation (Mein and Larson, 1971). The infiltration algorithm produced infiltration rate curves within a few percent of the Richards equation solution.

INDEPENDENT TESTING

Johnson *et al.* (1993) performed an independent calibration and verification of CASC2D on the Goodwin Creek experimental watershed in Mississippi. Calibration of CASC2D at the outlet of this basin was verified against stream flow gauging stations within the basin, for a total of five different runoff events. CASC2D was also compared with the Snyders Instantaneous Unit Hydrograph (SIUH) and SCS Curve Number (CN) approaches in HEC-1, using Muskingum-Cunge channel routing. These researchers concluded that CASC2D consistently performed as well or better than either the SIUH or CN HEC-1 approaches on the Goodwin Creek dataset. The primary calibration parameters used include initial soil moisture deficit, channel roughness coefficient, retention storage depth, and overland flow roughness coefficient. They also concluded that CASC2D always produced more accurate hydrographs on simulated ungauged basins (from the parametric values of Manning n and infiltration based on soil types without calibration).

STABILITY AND NUMERICAL ACCURACY

The stability of CASC2D was examined during the development (Saghafian, 1992; Julien and Saghafian, 1991). In summary, the explicit overland and channel flow algorithms require relatively small time steps for stability. The optimum time step depends upon the grid size, rainfall intensity, rainfall duration, both average and local bed slopes in the basin, surface roughness, and infiltration parameters. Specifically, the Courant condition evaluated under peak discharge conditions, which is the critical state with maximum flow velocity, provides a preliminary time

step value. The maximum time step for which the model is stable should be used because optimum solution convergence is achieved when the Courant number is near 1.0. Numerical stability is achieved on typical grid sizes with time steps between 5 and 60 seconds.

Situations which are particularly difficult to model with the CASC2D channel routing formulation include narrow channels with substantial changes in bed slope or channel cross-section. These can cause numerical instability in the transfer of water between the channel and floodplain during periods of over bank flow.

Surfaces with highly irregular microtopography at scales much smaller than the grid size do not pose a problem. Tayfur *et al.* (1993) found that replacing spatially varying microtopography with an average constant slope and appropriate retention storage causes no significant changes in the outflow hydrograph but does cause substantial deviations in local flow depths and velocities. Therefore, the user should be cautioned regarding the accuracy of flow velocity calculations within individual grid cells.

EXAMPLE APPLICATIONS OF CASC2D

The following two sections present example applications of CASC2D. The first section is an application of CASC2D with rainfall data from a dense raingauge network during a calibration run. The second section presents a brief discussion of contemporary weather radar rainfall rate estimation techniques and illustrates the applicability of weather radar estimated rainfall within CASC2D.

Modeling of Macks Creek Experimental Watershed with Raingauge Data

Macks Creek, a 32.2 km^2 sub-basin of the Reynolds Creek Experimental Watershed, is a steep semi-arid watershed located in southwest Idaho. A contour plot of Macks Creek is shown in Figure 3, with a 1 km grid overlay as a scale reference. The elevation drops from 1830m in the mountains along the western edge to 1130m at the outlet which is located in the northeast corner of the watershed. Two main channels, each

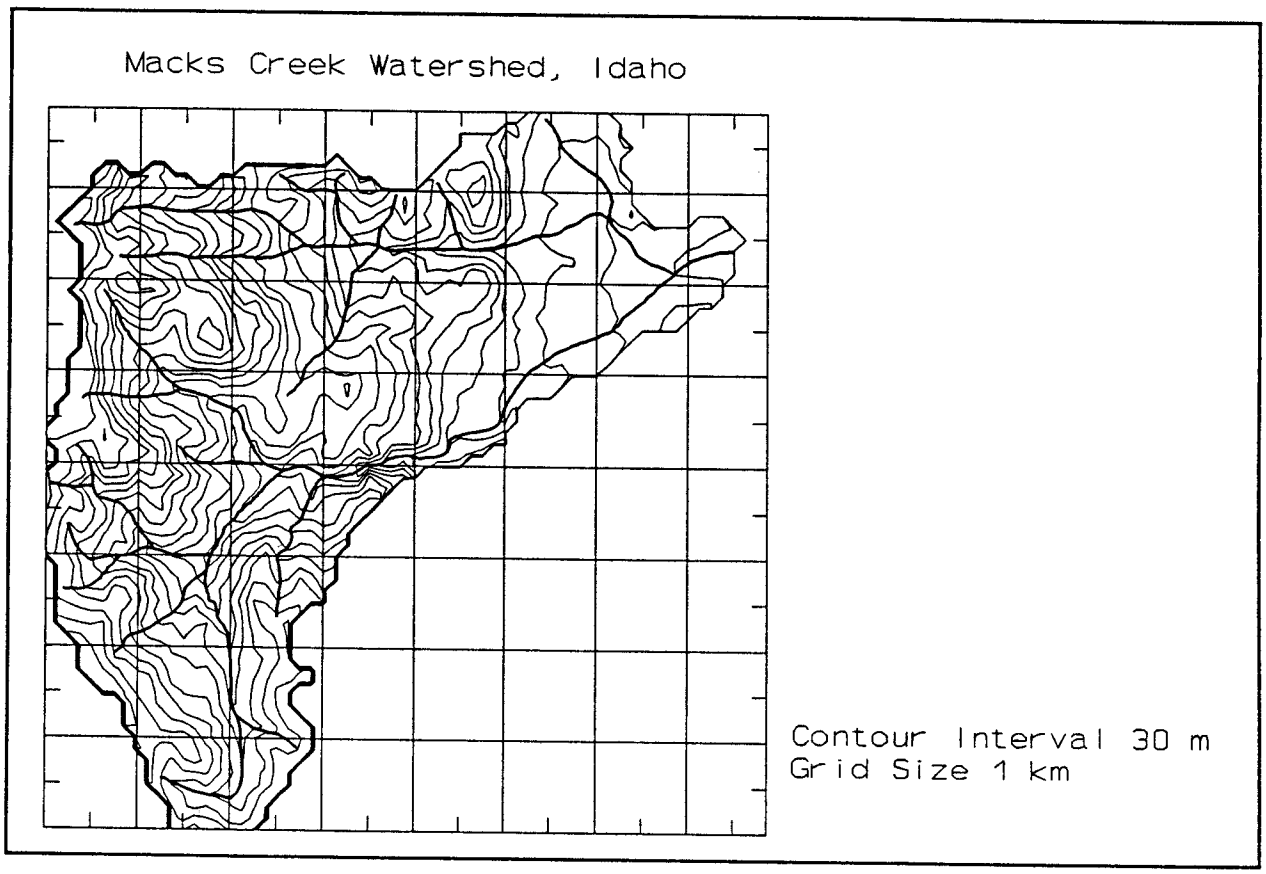

Figure 3. Macks Creek Watershed Topography and Channel Network.

with slopes averaging 5 percent and lengths near 10 km, collect surface runoff. The channel network is shown on Figure 3 with heavy lines. Note the longest continuous channel which drains the southern portion of the watershed and flows approximately from southwest to northeast. The second main channel drains the northern portion of the watershed, and flows in a roughly easterly direction.

For this particular calibration run the storm of August 23, 1965, was selected. Rainfall data with two-minute resolution was recorded by eight raingauges located on or near the watershed. The recorded accumulated rainfall depth over the two-hour storm reached 1.65 cm at one gauge, with a maximum rainfall rate over a two-minute period exceeding 20 cm/hr. Inverse distance squared weighting was applied to interpolate rainfall fields from the raingauge data. Outflows were recorded at a pre-calibrated 100 m^3/s capacity drop box weir at the watershed outlet on 15-minute intervals. A base flow of approximately 0.023 m^3/s at the outlet was neglected in the view of the 2.4 m^3/s measured peak discharge.

The geographical region containing the watershed was divided into a 53 x 53 grid, with a grid size of 152 m. The watershed mask contains 1390 grid cells. In this instance, the topography of Macks Creek was manually digitized to produce a raster DEM at a grid size of 152 m. The SCS soil classification map of Macks Creek was digitized by Cline (1988) at this same grid size. Both digitized maps were entered in the GRASS GIS for storage, editing, and export to CASC2D.

Values of hydraulic conductivity and capillary drive based on soil textural classification were used as recommended by Rawls *et al.* (1983). Antecedent soil moisture conditions were assumed near-dry owing to the semi-arid climate of the region, the absence of any substantial rainfall on the preceding day, and the negligible base flow at the weir. A spatially uniform value of Manning n for overland flow equal to 0.06 was used, which is within the range proposed by Woolhiser (1975) for sparse vegetation. The calibration parameters selected for this example are surface roughness and initial soil moisture deficit. Adequacy of this particular calibration was judged based on the timing and magnitude of the peak discharge, as well as the total runoff hydrograph volume.

Figure 4 shows the CASC2D visual display at 20, 35, 70, and 239.5 minutes during the model run. Each visual display is further broken down into sub-windows. The upper left sub-window shows the rainfall rate over the watershed, while the upper right sub-window depicts the surface water depth in each grid cell. The lower left and right sub-windows, respectively, display the cumulative infiltrated depth and the outflow hydrograph. The purple dots on the hydrograph sub-window represent observed discharge measurements at the weir.

With reference to the upper left quadrant of Figure 4, the storm is approaching the southeastern border of the watershed at t = 20 minutes. Note that at this point in the model run, the surface water depth is zero everywhere with the exception of a few rock outcrops along the western edge of the catchment. The classic "egg yolk" features in the interpolated rainfall field are the result of the inverse-distance squared rainfall interpolation scheme. Referring to the top right quadrant of Figure 4, at t = 35 minutes, the storm has moved to the northwest and intensified over the northeastern portion of the watershed. Accordingly, the cumulative infiltrated depth and surface water depth windows illustrate the partitioning of the rainfall into soil and surface water components. Note the partial areas of contribution in the surface water depth map.

As this particular storm unfolds, no surface runoff is generated from the southern third of the watershed. With reference to the lower left quadrant of Figure 4, at t = 70 minutes, there is no surface water in this portion of the watershed. At this time the hydrograph peak has just reached the catchment outlet. The short-duration high-intensity rainfall on the northern portion of the watershed is responsible for this sudden flashflood. In the lower right quadrant of Figure 4, at t = 239.5 minutes, all surface water is now limited to channel flow draining slowly toward the outlet. As evidenced by the hydrograph plot, fair agreement is observed between the computed hydrograph (solid red line) and the observed hydrograph (purple dots). Given the 15-minute temporal resolution of the recorded outflow hydrograph and the flashy response of Macks Creek, there is considerable uncertainty regarding the magnitude and timing of the measured hydrograph peak. Overall, this calibration run demonstrates that surface runoff is generated on partial areas of the watershed (northern part in this case). The model can accurately simulate surface runoff from flashfloods caused by intense thunderstorms moving across partial areas of a watershed.

Example Application of CASC2D with Weather Radar Estimated Rainfall

This section illustrates a CASC2D runoff simulation using real weather radar rainfall rates applied to a watershed at a different location. Weather radar observations of a convective storm over the plains of eastern Colorado are converted to rainfall rate estimates and used as input to CASC2D on the Macks Creek, Idaho, experimental watershed, which was discussed in the previous section. This simulation

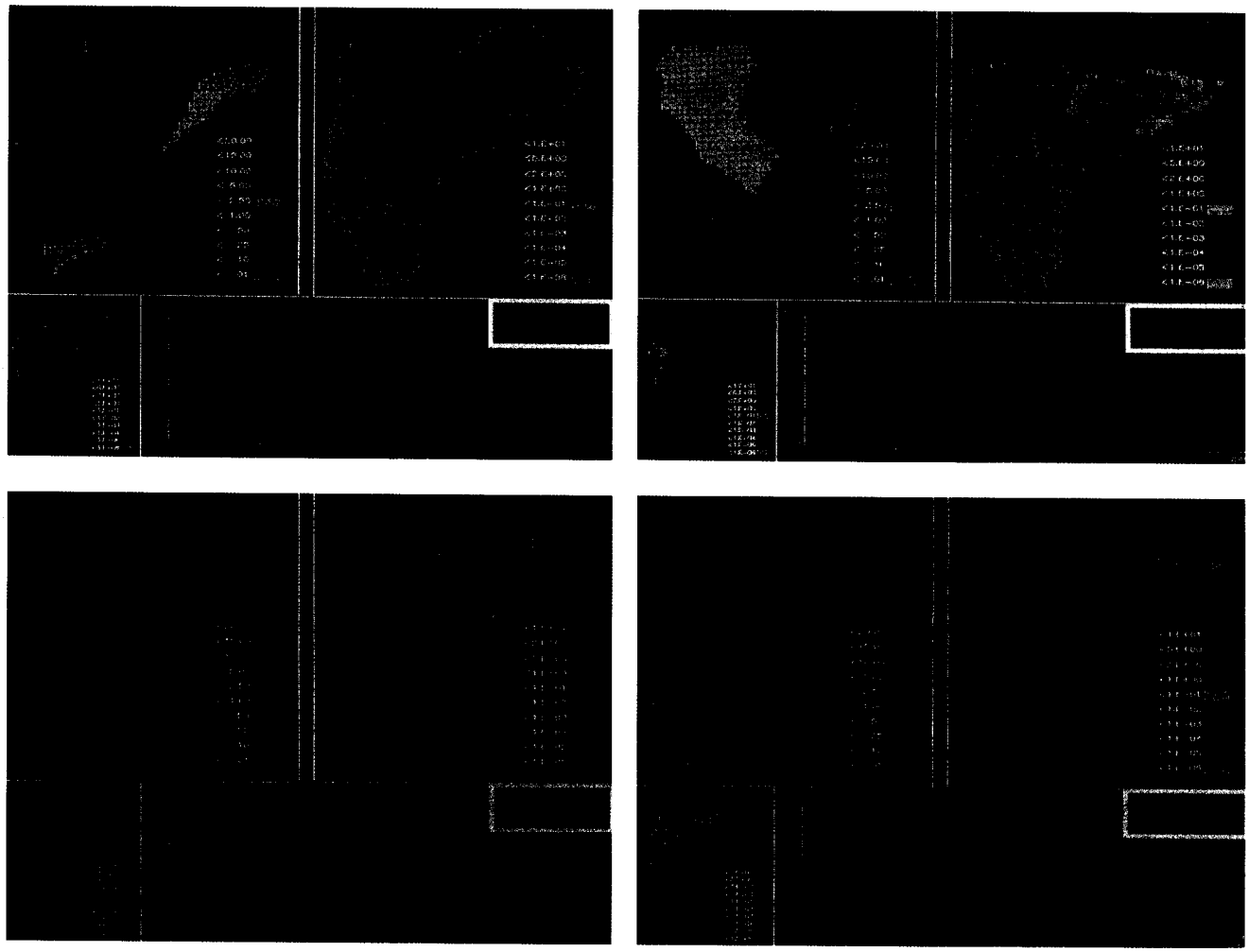

Figure 4. CASC2D Calibration on Macks Creek Using Raingauge Data at t = 20 Min. (upper left), 35 Min. (upper right), 70 Min. (lower left), and 239.5 Min. (lower right).

illustrates how CASC2D can interface with radar data, although, without comparison of the simulation results with an actual runoff hydrograph.

The raster formulation of CASC2D readily accepts raster estimates of rainfall rate at any spatial resolution. Raster rainfall estimates may be derived from interpolated raingauge data or isohyetal maps, weather radar or satellite observations, or space-time stochastic rainfall models. The only requirement is that the rainfall raster grid size must be evenly divisible by the runoff model grid size. For this reason, the elevation and soil classification maps of Macks Creek were re-digitized at a resolution of 125 m. Rainfall data grid size considerations and related scaling issues are discussed at length by Ogden and Julien (1994).

This example simulation relies upon CSU-CHILL weather radar observations of a convective rainstorm at five-minute intervals and 1 km spatial resolution. The CSU-CHILL radar is a research facility jointly funded by the National Science Foundation and Colorado State University. It operates at a non-attenuating wavelength of 10 cm (frequency = 2.95 GHz), has a 1 degree beam-width, and has dual-linear polarization and Doppler capabilities. For this example the radar measurements (Reflectivity, Differential Reflectivity, and Specific Differential Propagation Phase Shift) were converted into rainfall rate using the method detailed in Ogden and Julien (1994) and Ogden (1992). Readers interested in advanced radar-rainfall estimation techniques are referred to discussions by Zawadzki (1982), Sachidananda and Zrnic (1987), Chandrasekar *et al.* (1990, 1993), Gorgucci *et al.* (1994), and Aydin *et al.* (1995).

The CSU-CHILL radar monitored a convective storm on June 3, 1991. The radar measurements were

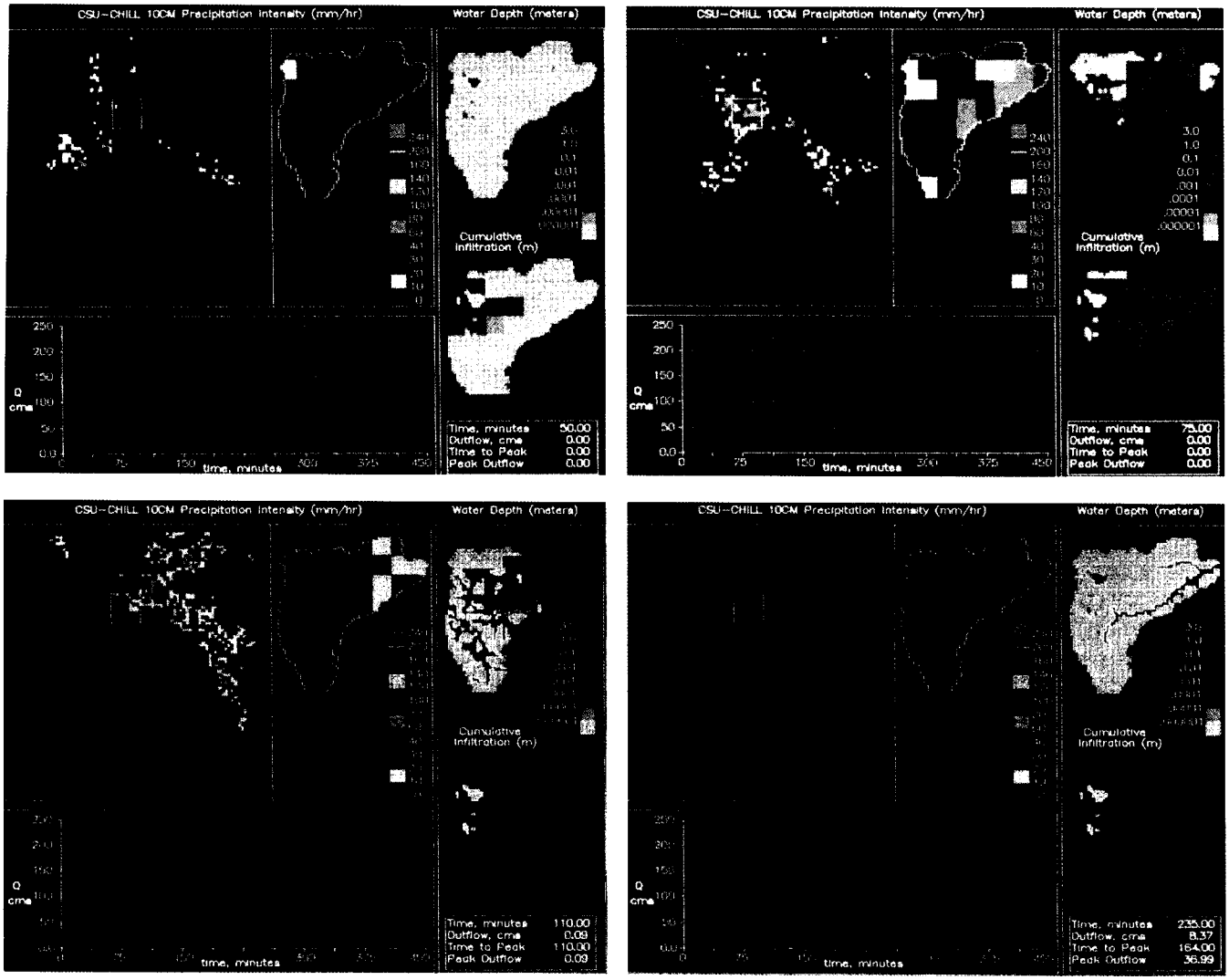

Figure 5. CASC2D Simulation on Macks Creek Using Weather Radar Estimated Rainfall at t = 50 Min. (upper left),75 Min. (upper right), 110 Min. (lower left), and 235 Min. (lower right).

recorded in spherical coordinates, with 300 m spatial resolution in the direction of the radar beam, and 1 degree resolution in the azimuthal and elevation angle directions. Radar scans at a beam elevation angle of 1 degree above the horizon were completed once per five minutes over the duration of the storm, which lasted about 150 minutes. After conversion to rainfall rates in spherical radar coordinates, the rainfall estimates were converted onto a 1 km x 1 km raster grid using a minimum-curvature spline technique.

Similar to Figure 4, Figure 5 shows a visual display of CASC2D with weather radar estimated rainfall at four different times during the simulation (50, 75, 110, and 235 minutes respectively). The CASC2D graphical display with radar-estimated rainfall is different from the display with raingauge rainfall. Specifically, the upper-left sub-window was added to illustrate the spatial variability of rainfall within a large radar domain around the watershed, which is 80 x 80 km in size. The location of the watershed within this sub-window is bounded by a white rectangle, and the radar is located near the center of the sub-window. For this illustrative example, the location of the watershed within the radar domain was chosen arbitrarily.

With reference to the visual display shown in the upper left quadrant of Figure 5, at simulation time t = 50 minutes after the beginning of simulation, the storm can be seen building west of the watershed location in the radar domain sub-window. The spatial variability of the 1 km raster rainfall field over the watershed is shown in the upper-middle sub-window. The light blue pixel in the watershed rainfall

sub-window indicates a rain rate between 30 and 40 mm/h on the very western edge of the basin. The upper-right and lower-right sub-windows detail the surface water and cumulative infiltrated depths, respectively, at this point in the simulation. Note the similarity with the graphical displays in Figure 4 with regard to the rocky outcrops along the western edge of the watershed. The surface depth map indicates ponded conditions on the rocky areas while the cumulative infiltrated depth map indicates no infiltration.

Referring to the upper right quadrant of Figure 5, at t = 75 minutes, the convective storm can be seen directly over the watershed in the upper left sub-window. The upper-middle sub-window shows one 1 km x 1 km region (yellow rainfall pixel) receiving an estimated rainfall rate between 120 and 140 mm/h. The upper right sub-window shows that the overland flow in the southwestern portion of the watershed is beginning to accumulate in the channel network, while the lower right sub-window shows a significant increase in infiltrated depth, particularly in the northeastern corner of the watershed, where it is now raining most heavily. The hydrograph display and simulation summary box in the lower portion of the video display indicate that runoff has not yet reached the outlet.

The video display in the lower-left quadrant of Figure 5 shows the state of the simulation at t = 110 minutes. As seen in the radar domain sub-window, the bulk of the storm has passed east of the watershed location. The upper-middle sub-window shows that rainfall rates less than 30 mm/h continue to fall in the extreme northeast corner of the watershed, while light rainfall less than 10 mm/h covers the central portion of the catchment. The surface depth map shows significant accumulations of water in the channel network with a flood wave moving toward the outlet in each of the two main channels. The cumulative infiltration map shows significant cumulative infiltration in the middle and eastern portions of the watershed, while the simulation status box in the extreme lower-right corner indicates the present outflow rate is 0.09 m^3/s.

The lower right quadrant of Figure 5 shows the CASC2D visual display at a simulation time of 235 minutes. The radar domain sub-window indicates no precipitation in the area or on the watershed. The surface water depth sub-window shows that all surface waters have infiltrated except in some channels, floodplains, and rocky regions. Furthermore, this window shows that the flood waves from both main channels have passed through to the outlet. The resulting hydrograph from this storm is shown in the lower-left sub-window, and the simulation summary sub-window indicates a peak discharge of 36.99 m^3/s passed the outlet at t = 184 minutes. Note the degree of spatial detail available at the end of the simulation regarding the location of flood waters, and spatial variability of cumulative infiltrated depth. This information could be most useful for the initiation of a new simulation if a second storm were to be headed toward the watershed.

SUMMARY AND CONCLUSIONS

Recent developments and increasing usage of GIS technology for the storage and retrieval of watershed characteristics in raster format enhance hydrological models that can fully access these data sources. GIS technology has also shown the educational, scientific, and diagnostic value of visual displays of large data sets. Furthermore, the increasing availability of weather radar rainfall estimates in raster format also necessitates the development of hydrological models capable of incorporating spatially-varied rainfall while preserving the spatial and temporal information provided by weather radars.

This paper outlines the details of the model formulation and list assumptions pertaining to the development and verification of the components. The calibration and accuracy of CASC2D are discussed together with numerical stability and model limitations. Two example applications which simulate the response of the 32.2 km^2 Macks Creek experimental watershed in southwestern Idaho are presented. The first application illustrates a CASC2D calibration run with rainfall rates interpolated from a dense network of raingauges. The second example illustrates the link between CASC2D and radar-estimated rainfall. In both examples, the utility of the graphical display in relating the state of a simulation to the user is discussed.

The accuracy of the overland flow, infiltration, and channel routing components of CASC2D has been assessed independently. CASC2D produces runoff hydrographs which are generally more accurate than either the SCS CN or Snyders Instantaneous Unit Hydrograph approaches with Muskingum Cunge channel routing in HEC-1. The unique visual display capability of CASC2D allows the user unprecedented access to the entire simulation while it is in progress. The visual display essentially provides CASC2D users access to the results of the simulation as it unfolds. This capability has potential for practical as well as research applications. The model is particularly well-suited to the simulation of flashfloods from intense thunderstorms moving across partial areas of a watershed.

In conclusion, the physically-based distributed nature of CASC2D makes it a suitable modeling tool to carry out fundamental research on spatially-varied systems. CASC2D features include GIS compatibility, direct link with remotely-sensed rainfall data, accuracy of simulation, and unique graphical interface. The paper presents innovative applications of recent advances in computational hydrology. As illustrated in Figure 4, the model can accurately simulate surface runoff from flashfloods caused by intense thunderstorms moving across partial areas of a watershed.

ACKNOWLEDGMENTS

This study was completed at the Engineering Research Center within the Center for Excellence in Geosciences at Colorado State University. Financial support by the U.S. Army Research Office (Grant ARO/DAAL 03-86-0175) is gratefully acknowledged. We appreciate the technical assistance of Drs. J. S. O'Brien, W. Doe III, O. R. Stein, Y. Q. Lan, K. Marcus, and G. Choi at the time the model was developed. Our gratitude is extended to Dr. W. Bach for his continuous support of this research program.

LITERATURE CITED

Abbott, M. B., J. C. Bathurst, J. A. Cunge, P. E. O'Connell, and J. Rasmussen, 1986. An Introduction to the European Hydrological System – Système Hydrologique Européen, "SHE." 2: Structure of a Physically-Based, Distributed Modelling System, Journal of Hydrology 87:61-77.

Aydin, K., V. N. Bringi, and L. Liu, 1995. Rain Rate Estimation in the Presence of Hail Using S-band Specific Differential Phase and Other Radar Parameters, Journal Appl. Meteorol. 34(2) (In Press).

Chandrasekar, V., V. N. Bringi, N. Balakrishnan, and D. S. Zrnic, 1990. Error Structure of Multiparameter Radar and Surface Measurements of Rainfall. Part III: Specific Differential Phase. Journal Atmos. Oceanic Technol. 7(5):621-629.

Chandrasekar, V., E. Gorgucci, and G. Scarchilli, 1993. Optimization of Multiparameter Radar Estimates of Rainfall. Journal Appl. Meteorol. 32(7):1288-1293.

Choi, G. W. and A. Molinas, 1993. Simultaneous Solution Algorithm for Channel Network Modeling. Water Resources Research 29(2):321-328.

Cline, T. J., 1988. Development of a Watershed Information System for HEC-1 with Application to Macks Creek, Idaho. M.S. Thesis, Civil Engineering Dept., Colorado State University, Fort Collins, Colorado, 238 pp.

Cline, T. J., A. Molinas, and P. Julien, 1989. An Auto-CAD-Based Watershed Information System for the Hydrologic Model HEC-1. Water Resources Bulletin, 25(3), pp. 641-652.

DeVantier, B. A. and A.D. Feldman, 1993. Review of GIS Applications in Hydrologic Modeling. Journal of Water Resources Planning and Management, ASCE, 119(2):246-261.

Dickinson, W. T., M. E. Holland, and G. L. Smith, 1967. An Experimental Rainfall-Runoff Facility. Hydrology Paper No. 25, Colorado State University, Fort Collins, Colorado.

Doe, W. W., 1992. Simulation of the Spatial and Temporal Effects of Army Maneuvers on Watershed Response. Ph.D. Dissertation, Civil Engineering Dept., Colorado State University, Fort Collins, Colorado, 301 pp.

Doe, W. W. and B. Saghafian, 1992. Spatial and Temporal Effects of Army Maneuvers on Watershed Response: The Integration of GRASS and a 2-D Hydrologic Model. Proc. 7th Annual GRASS Users Conference, National Park Service Technical Report NPS/NRG15D/NRTR-93/13, Lakewood, Colorado, pp. 91-165.

Goodrich, D. C., D. A. Woolhiser, and T. O. Keefer, 1991. Kinematic Routing Using Finite Elements on a Triangular Irregular Network. Water Resources Research 27(6):995-1003.

Gorgucci, E., G. Scharchilli, and V. Chandrasekar, 1994. A Robust Pointwise Estimator of Rainfall Rate Using Differential Reflectivity. Journal Atmos. Oceanic. Tech. 11(2):586-592

James, W. P. and K. W. Kim, 1990. A Distributed Dynamic Watershed Model. Water Resources Bulletin 26(4):587-596.

Johnson, B. E., N. K. Raphelt, and J. C. Willis, 1993. Verification of Hydrologic Modeling Systems. Proc. Federal Water Agency Workshop on Hydrologic Modeling Demands for the 90's, USGS Water Resources Investigations Report 93-4018, June 6-9, Sec. 8., pp. 9-20.

Julien, P. Y. and B. Saghafian, 1991. A Two-Dimensional Watershed Rainfall-Runoff Model. Civil Engr. Report, CER90-91PYJ-BS-12, Dept. of Civil Engineering, Colorado State University, Fort Collins, Colorado, 63 pp.

Klazura, G. E. and D. A. Imy, 1993. A Description of the Initial Set of Analysis Products Available from the NEXRAD WSR-88D System. Bull. Am. Meteor. Soc., 74(7):1293-1311.

Marcus, K. B., 1991. Two-Dimensional Finite Element Modeling of Surface Runoff from Moving Storms on Small Watersheds. Ph.D. Dissertation, Civil Engineering Dept., Colorado State University, Fort Collins, Colorado.

Mein, R. G. and C. L. Larson, 1971. Modeling the Infiltration Component of the Rainfall-Runoff Process. Bulletin 43, Water Resources Research Center, University of Minnesota, Minneapolis, Minnesota.

Ogden, F. L., 1992. Two-Dimensional Runoff Modeling with Weather Radar Data. Ph.D. Dissertation, Civil Engineering Dept., Colorado State University, Fort Collins, Colorado., 211 pp.

Ogden, F. L. and P. Y. Julien, 1993. Runoff Sensitivity to Temporal and Spatial Rainfall Variability at Runoff Plane and Small Basin Scales. Water Resources Research 29(8):2584-2597.

Ogden, F. L. and P. Y. Julien, 1994. Runoff Model Sensitivity to Radar-Rainfall Resolution. Journal of Hydrology 158:1-18.

Rawls, W. J., D. L. Brakensiek, and N. Miller, 1983. Green-Ampt Infiltration Parameters from Soils Data. Journal of Hydraulic Engineering, ASCE 109(1):62-70.

Sachidananda, M. and D. S. Zrnic , 1987. Rain Rate Estimates from Differential Polarization Measurements. Journal of Atmos. and Oceanic Tech 4:588-596.

Saghafian, B., 1992. Hydrologic Analysis of Watershed Response to Spatially Varied Infiltration. Ph.D. Dissertation, Department of Civil Engineering, Colorado State University, Fort Collins, Colorado.

Schaake, J. C., 1965. Synthesis of the Inlet Hydrograph. Ph.D. Dissertation, Dept. of Sanitary Engineering and Water Resources, The Johns Hopkins University, Baltimore, Maryland.

Tayfur, G., M. L. Kavvas, R. S. Govindaraju, and D. E. Storm, 1993. Applicability of St. Venant Equations for Two-Dimensional Overland Flows Over Rough Infiltrating Surfaces. Journal of Hydraulic Engineering, ASCE 119(1):51-63.

Vieux, B. E., 1991. Geographic Information Systems and Non-Point Source Water Quality and Quantity Modeling. Hydrological Processes 5:101-113.

Woolhiser, D. A., 1969. Overland Flow on a Converging Surface. Trans. of ASAE, 12(4):460-462.

Woolhiser, D. A., 1975. Simulation of Unsteady Overland Flow. *In:* Unsteady Flow in Open Channels, Vol. II, Chapter 12, K. Mahmood and V. Yevjevich (Editors). Water Resources Publications, Fort Collins, Colorado.

Zawadzki, I, 1982. The Quantitative Interpretation of Weather Radar Measurements. Atmos. Ocean 20:158-180.

Zhang, W. and T. W. Cundy, 1989. Modeling of Two-Dimensional Overland Flow. Water Resources Research 25(9):2019-2035.

NOTATIONS

E = ground elevation
f = infiltration rate
F = cumulative infiltration depth
g = gravitational acceleration
h = flow depth
H_f = capillary pressure head at the wetting front
i = rainfall intensity
i_e = excess rainfall intensity
j = row number of grid cell
k = column number of grid cell
L = total length along hydraulically longest kinematic flow path
M_d = soil moisture deficit
n = Manning roughness coefficient
q = unit discharge
q_l = lateral inflow
q_x, q_y = unit discharge in the x,y directions
Q = total discharge
R = hydraulic radius
S = degree of initial soil saturation
S_o = bed slope
S_f = friction slope
t = time
V = flow velocity
W = overland plane width
x,y = Cartesian coordinates
α_x, β, γ = parameters of the resistance equations
θ_e = the effective soil porosity
θ_i = initial soil moisture content
θ_r = residual saturation
ϕ = total soil porosity